

CrystEngComm

Accepted Manuscript



This is an *Accepted Manuscript*, which has been through the Royal Society of Chemistry peer review process and has been accepted for publication.

Accepted Manuscripts are published online shortly after acceptance, before technical editing, formatting and proof reading. Using this free service, authors can make their results available to the community, in citable form, before we publish the edited article. We will replace this *Accepted Manuscript* with the edited and formatted *Advance Article* as soon as it is available.

You can find more information about *Accepted Manuscripts* in the [Information for Authors](#).

Please note that technical editing may introduce minor changes to the text and/or graphics, which may alter content. The journal's standard [Terms & Conditions](#) and the [Ethical guidelines](#) still apply. In no event shall the Royal Society of Chemistry be held responsible for any errors or omissions in this *Accepted Manuscript* or any consequences arising from the use of any information it contains.

Cite this: DOI: 13.1039/c0xx00000x

www.rsc.org/xxxxxx

ARTICLE TYPE

A family of 3D UO_2^{2+} -5-X-1,3-dicarboxylate ($X = -\text{H}, -\text{NO}_2, -\text{NH}_2, -\text{OH}$) hybrid materials: structural relevance with a variation of substituent group and photochemical properties

Xiang-Sheng Zhai, Wen-Gang Zhu, Wei Xu, Ya-Jing Huang, Yue-Qing Zheng*

5 Received (in XXX, XXX) Xth XXXXXXXXX 2014, Accepted Xth XXXXXXXXX 2014

DOI:

Four new 3D uranyl complexes, $[(\text{UO}_2)_2(\text{H}_2\text{O})(\text{ipa})_2] \cdot 9\text{H}_2\text{O}$ (**1**), $[(\text{UO}_2)_2(\text{H}_2\text{O})(\text{nip})_2] \cdot \text{H}_2\text{O} \cdot \text{Et}_3\text{NH}$ (**2**), $[(\text{UO}_2)_2(\text{H}_2\text{O})(\text{aip})_2] \cdot \text{Et}_3\text{NH}$ (**3**) and $[(\text{UO}_2)_2(\text{hip})_2] \cdot 17\text{H}_2\text{O}$ (**4**) (H_2ipa = isophthalic acid, H_2nip = 5-nitroisophthalic acid, H_2aip = 5-aminoisophthalic acid, H_2hip = 5-hydroxyisophthalic acid, Et_3N = triethylamine), were hydrothermally synthesized. Structural analyses reveal that Compound **1–4** consist of pentagonal bipyramidal uranyl monomers bridged *via* acid linkers to form a structural motif, $[(\text{UO}_2)_2\text{L}_2]$, serving as the foundation for the 3D framework. Two structural motifs adopt different arrangement mode to connect to two types of chains. For **1–3**, uranium atoms and carboxyl groups being from two types of chains respectively are coordinated to build the similar 3D frameworks, while for **4**, one type of chain links to 3D architecture by the bond of the uranium atoms and $-\text{OH}$ of 5-hydroxyisophthalic acid ligands. The different guest molecules and structure assembling displayed throughout four compounds is a function of the variation of substituent groups for 5-X-1,3-benzenedicarboxylic acid ($X = -\text{H}, -\text{NO}_2, -\text{NH}_2, -\text{OH}$). Furthermore, the photocatalytic properties of **2** and **4** for degradation of the rhodamine-B (RhB) upon xenon lamp irradiation have been examined. Elemental analysis, infrared spectroscopy, DRS and luminescence properties were also discussed.

Introduction

In recent years, the rapid growth of the field of uranyl-containing hybrid materials is largely motivated by the vast array of structural variation afforded by the combinations of organic ligands and the uranyl cation, UO_2^{2+} [1]. Uranyl-bearing materials afford the opportunity to explore uranium-organic interactions beyond structural interests, and as such there is an implied synergy between materials synthesis and studies of uranyl speciation and complexation from an analytical or environmental perspective. Generally, the local geometry of the uranyl cation, a linear triatomic species capped with terminal oxygen atoms, would influence the structures of uranyl hybrid materials, tending to restrict ligand coordinated to the equatorial plane and induce three primary building units, namely, square, pentagonal, and hexagonal bipyramids, in the solid state [2]. Additionally, UO_2^{2+} is susceptible to hydrolysis and therefore may promote the formation of secondary building units (dimers, trimers, sheets, etc.), which provides a metal-centered route toward increasing topological diversity of uranyl hybrid materials [3].

Traditional organic ligands utilized in uranyl hybrid material synthesis contain carboxylic acid or phosphoric acid groups as per their affinity for UO_2^{2+} [1b–1e,4]. The structural variation of hybrid materials is further contributed to the modification of the

organic component. Meanwhile, the network structure of coordination polymer can be thought of as assembly of the organic ligand possessing some connection nets and metal ions. Thus geometric configurations of ligands and coordination geometry of metal ions have significant influence to the network structure of coordination polymer [5]. And the overall structure can be predicted by the geometrical shape of ligand molecules and the coordination geometry of metal ions.

Ligand influence on coordination polymer can be summarized to the quantity and property of the coordination sites, the distance between the coordination sites, the geometric configurations of ligands and the template of ligands. The structures and properties of coordination polymer synthesized can be controlled by selecting organic ligands. Ligands control the size of the cavity in the network structure, exerting an influence on the properties of coordination polymer, such as catalytic. Thus, to modify the organic component, the substituent groups of ligands play a decisive influence on the properties and functional of coordination polymer [6].

To investigate the substituent effects on the structure and properties, the organic ligand 5-X-1,3-benzenedicarboxylic acid ($X = -\text{H}, -\text{NO}_2, -\text{NH}_2, -\text{OH}$) (Scheme 1) features both aforementioned sites and therefore is an attractive organic ligand for such an approach. The use of the title ligands are inspired by 1,3,5-benzenetricarboxylic acid [7], wherein two (of three)

carboxylates show direct coordination to UO_2^{2+} and one remains varying to form acid ligands possessing different substituent groups. Additionally, the study about uranyl hybrid materials using 5-X-1,3-benzenedicarboxylic acid is interesting and significant for the varied structures and properties^[14,15].

Herein we present four new hydrothermally synthesized uranyl hybrid materials incorporating 5-X-1,3-benzenedicarboxylic acid: $[(\text{UO}_2)_2(\text{H}_2\text{O})(\text{ipa})_2] \cdot 9\text{H}_2\text{O}$ (**1**), $[(\text{UO}_2)_2(\text{OH})(\text{nip})_2] \cdot \text{H}_2\text{O} \cdot \text{Et}_3\text{NH}$ (**2**), $[(\text{UO}_2)_2(\text{OH})(\text{aip})_2] \cdot \text{Et}_3\text{NH}$ (**3**) and $[(\text{UO}_2)_2(\text{hip})_2] \cdot 17\text{H}_2\text{O}$ (**4**). We focus on the resulting local and global structures of **1–4** as influenced by substituent groups on the organic linker and to a lesser extent the effect of structure directing agents. The structural variations within these compounds also prompted a property investigation to explore any relationship between topology and uranyl emission. Compounds **2** and **4** with the band-gap sizes of 2.12 eV and 2.20 eV all display interesting photocatalytic properties on the degradation of organic dyes rhodamine B (RhB) under simulate daylight irradiation of xenon lamp.

20 Experimental Section

Materials and physical Methods

Caution! Whereas the uranyl acetate dihydrate $\text{UO}_2\text{Ac}_2 \cdot 2\text{H}_2\text{O}$ used in these experiments contained depleted uranium, standard precautions for the handling and disposal of radioactive materials should be observed.

All chemicals of reagent grade were commercially available and used without further purification. Uranyl acetate (99.8%, HuBei ChuShengWei Chemistry Reagent Co. Ltd.), H_2ipa , H_2nip , H_2aip , and H_2hip (99%, ShangHai Aladdin Reagent Co. Ltd.) are listed in Scheme 1. The reaction mixtures were loaded into a 23 mL Teflon-lined stainless steel autoclave. The autoclave was sealed and heated at 140 °C for 3 days, and then cooled to room temperature naturally. The single crystals were isolated for all of the title compounds. Single crystal X-ray diffraction data were collected by Rigaku Raxis-Rapid X-ray diffractometer. Powder X-ray diffraction (PXRD) patterns were carried out with a Bruker D8 Focus X-ray diffractometer with Cu $K\alpha$ radiation ($\lambda = 0.15405$ nm, continuous, 40 kV, 40 mA, increment = 0.02°) to identify the synthetic products as well as to check phase purity. The C, H and N microanalyses were performed with a PE 2400II CHNO/S elemental analyzer. All FT-IR spectra were recorded at room temperature on a Shimadzu FTIR-8900 spectrometer. Samples were diluted with spectroscopic KBr and pressed into a pellet. Scans were run over the range 400–4000 cm^{-1} . Differential thermal analyses (DTA) and thermogravimetric (TG) measurements, using a Seiko Exstar 6000 TG/DTA6300 apparatus, were conducted from room temperature to 900 °C on preweighed samples in flowing nitrogen with a heating rate of 10 °C/min. The fluorescence spectra were performed on a SHIMADZU RF-5301PC spectrofluorophotometer. The diffuse reflectance spectroscopy (DRS) spectra were recorded by a DR-UV-Vis spectrometer Lambda 950, and the wavelength ranges from 200 to 1000 nm. Photocatalytic tests were performed with Bilon BL-GHX-V photochemical reactions instrument.

55 Synthesis of $[(\text{UO}_2)_2(\text{H}_2\text{O})(\text{ipa})_2] \cdot 9\text{H}_2\text{O}$ (**1**)

In a typical synthetic procedure, 0.4241 g (1.0 mmol) uranyl acetate dehydrate and 0.1661 g (1.0 mmol) isophthalic acid were successively added to a stirred 18 mL aqueous solution, and then 0.14 mL (1.0 mmol) triethylamine was dropped. The mixture (pH = 5.2) was homogenized by stirring for 15 min and then transferred to a 23 mL Teflon-lined stainless-steel autoclave. The sealed reactor was heated at 140 °C for 3 days. After cooling to room temperature (pH = 4.5), few single crystals suitable for X-ray diffraction were isolated. Anal. Calc. for $\text{C}_{16}\text{H}_{10}\text{O}_{13}\text{U}_2$: C, 21.68; H, 1.14. Found: C, 21.35; H, 1.28%. IR data (cm^{-1} , KBr): 3059(w), 2984(w), 2723(w), 1607(m), 1599(m), 1547(s), 1535(s) 1479(s), 1460(s), 1408(vs), 1163(w), 1076(w), 920(vs), 837(m), 748(m), 717(s), 669(m), 582(w), 532(m), 498(m), 415(s) (Fig. S2).

70 Synthesis of $[(\text{UO}_2)_2(\text{OH})(\text{nip})_2] \cdot \text{H}_2\text{O} \cdot \text{Et}_3\text{NH}$ (**2**)

A synthetic procedure similar to that for **1** was employed. The reaction mixture is formed by uranyl acetate dehydrate (0.4241 g, 1.0 mmol), 5-nitroisophthalic acid (0.2111 g, 1.0 mmol), triethylamine (0.14 mL, 1.0 mmol) and deionized water (18 mL). The solution pH was 5.4 before the reaction and 4.8 at the end. The yellow crystalline products are obtained. Anal. Calc. for $\text{C}_{22}\text{H}_{25}\text{N}_3\text{O}_{18}\text{U}_2$: C, 24.12; H, 2.30; N, 3.97. Found: C, 23.95; H, 2.24; N, 4.12%. IR data (cm^{-1} , KBr): 3610(w), 3371(m), 3092(m), 1624(s), 1599(s), 1599(s), 1556(s), 1531(s), 1462(s), 1389(vs), 1348(s), 1113(w), 1088(w), 937(s), 920(s), 843(w), 822(w), 785(m), 733(s), 708(s), 615(m), 548(m) (Fig. 2S).

Synthesis of $[(\text{UO}_2)_2(\text{OH})(\text{aip})_2] \cdot \text{Et}_3\text{NH}$ (**3**)

The mixture is comprised of uranyl acetate dehydrate (0.4241 g, 1.0 mmol), 5-aminoisophthalic acid (0.1811 g, 1.0 mmol), triethylamine (0.14 mL, 1.0 mmol) and deionized water (18 mL). The solution pH was 5.0 before the reaction and 4.4 at the end. After filtration, few yellow rhombus crystals were obtained. Anal. Calc. for $\text{C}_{22}\text{H}_{28}\text{N}_3\text{O}_{13}\text{U}_2$: C, 26.07; H, 2.78; N, 4.15. Found: C, 25.93; H, 2.55; N, 4.06%. IR data (cm^{-1} , KBr): 3371(s), 1630(m), 1618(m), 1562(m), 1528(s), 1472(s), 1400(vs) 1117(w), 1003(w), 930(m), 905(s), 808(m), 771(m), 739(s), 721(m), 669(m), 613(w), 521(m), 434(m) (Fig. S2).

Synthesis of $[(\text{UO}_2)_2(\text{hip})_2] \cdot 17\text{H}_2\text{O}$ (**4**)

The reaction mixture consists of uranyl acetate dehydrate (0.4241 g, 1.0 mmol), 5-hydroxyisophthalic acid (0.2111 g, 1.0 mmol), triethylamine (0.14 mL, 1.0 mmol) and deionized water (18 mL). The solution pH values before and after the reaction are 5.1 and 3.1. After filtration, the large orange rhombus crystals were obtained. The orange rhombic crystals were obtained. Yield: 0.3984 g (87% based on uranium). Anal. Calc. for $\text{C}_{16}\text{H}_{10}\text{O}_5\text{U}_2$: C, 20.93; H, 1.10. Found: C, 21.15; H, 1.11. IR data (cm^{-1} , KBr): 3512(w), 3331(w), 3063(m), 2982(m), 2808(w), 2698(w) 1612(s), 1587(s), 1562(s), 1518(s), 1460(s), 1429(vs), 1387(vs), 1290(s), 1134(m), 1103(w), 1009(s), 984(m), 895(s), 797(s), 785(s), 717(s), 602(m), 527(w), 453(m), 426(m) (Fig. 2S).

X-ray Crystallography

Suitable single crystals were selected under a polarizing microscope and fixed with epoxy cement on the fine glass fibers, which were then mounted on a Rigaku R-Axis Rapid IP X-ray diffractometer with graphite-monochromated Mo K_{α} radiation ($\lambda = 0.71073$) for cell determination and subsequent data collection. The data were corrected for Lp and absorption effect. The SHELXS-97 and SHELXL-97 programs were used for structure solution and refinement^[8]. The structures were solved by using direct method, and the subsequent difference Fourier synthesis gave the positions of all non-hydrogen atoms. Three disordered methylene carbon atoms of triethylamine molecule in **3** were modeled with partial occupancies and anisotropic thermal parameters; their occupancies were allowed to refine freely in early stages of the refinement and then were fixed. After several cycles of refinement, all hydrogen atoms of organic ligands were geometrically generated, and the remaining hydrogen atoms were located from the successive difference Fourier syntheses. Finally, the full matrix least-squares technique was used to refine all non-hydrogen atoms with anisotropic displacement parameters and the hydrogen atoms with isotropic displacement parameters set to 1.2 times those of their carrier atoms. A very large void is located around (0.499, 0.499, 0.510) for **1** and (-0.009, -0.010, -0.012) for **2** in which large Fourier-difference peaks are located. The program SQUEEZE (PLATON)^[9] has been used to model this part of the structure. For **1**, about 184 electrons have been found in the 525 Å³ void, and removed 9 water molecules per formula unit, for **4**, the SQUEEZE calculations showed a total solvent accessible area volume of 1919 Å³ and the residual electron density amounted to 626 e per unit cell, and removed 16 water molecules per formula unit. The species occupying this position is seemingly highly disordered molecules, which could not be modeled as discrete atomic sites. Detailed information about the data collection and structure determination are summarized in Table 1. Selected interatomic distances and bond angles are given in Tables S1–S4.

Photocatalytic activity measurements

The photocatalytic activities of as-prepared samples were evaluated by the degradation of rhodamine B (RhB) under visible light irradiation of a 700/500/300 W Xe lamp. In a typical process, eight copies 8 mg complex were suspended in eight copies 30 mg/L RhB aqueous solution (pH = 5.9) 10 mL in tubes respectively, then magnetically stirred in the dark for about 30 min to ensure the establishment of an adsorption/desorption equilibrium. After that, the mixtures were stirred and continuously exposed to simulate daylight irradiation from a 500 W high pressure xenon lamp. A sample was continually taken from the reaction cell and collected by centrifugation at 20 min intervals during the irradiation, and subsequently the liquid supernatant was analyzed by SHIMADZU 2501PC UV-vis recording spectrophotometer.

Results and Discussion

Description of the Crystal Structures.

$[(\text{UO}_2)_2(\text{H}_2\text{O})(\text{ipa})_2] \cdot 9\text{H}_2\text{O}$ (**1**). Within the asymmetric unit

of **1** exists two independent uranyl cations, two isophthalate anions (denoted as L1 and L2 ligands, which contains O3 and O12, respectively) and one aqua ligand. As depicted in Fig 1a, the U1 atom is coordinated by two uranyl oxygen atoms (O1, O2), two oxygen atoms (O3, O4) of chelating bidentate carboxylates from L1, three oxygen atoms (O5^{#3}, O6^{#5}, O12) of bridging carboxylates from three L²⁻ (L1, L1, L2) to form pentagonal bipyramidal chromophore with $d(\text{UO}_2-\text{O}) = 2.305\text{--}2.459$ Å (Table S1). While the U2 atom is pentagonal bipyramidally coordinated by two uranyl oxygen atoms (O7, O8), two oxygen atoms (O10, O11) of chelating bidentate carboxylates and one oxygen atom (O13^{#2}) of bridging carboxylates from L2, and two aqua O atoms (O9, O9^{#1}) with $d(\text{UO}_2-\text{O}) = 2.316\text{--}2.459$ Å (Table S1). The above values correspond to the normal values reported in literatures^[10]. The two types of ipa²⁻ anions are all in a $\mu_3\eta^4$ coordination mode (type a in Scheme 2) chelating one U atom in a normal manner through one carboxylate and bridging two U atoms. Two adjacent U2 atoms are connected by two aqua ligands to form the edge-sharing equatorial oxygen atoms of dinuclear uranyl unit $[(\text{UO}_2)_2(\text{H}_2\text{O})_2]^{4+}$. The resulting dinuclear units are further bridged by four $\mu_3\eta^4\text{-}\kappa\text{O}:\kappa^2\text{O},\text{O}'$ ipa²⁻ anions to form a 1D ribbon-like chain (chain2) along the [110] direction in terms of $\left\{[(\text{UO}_2)_2(\text{H}_2\text{O})_2]\text{ipa}_2\right\}$ with a bindingless carboxyl oxygen atom O12 (Fig. 2b). While the same coordination mode of ipa²⁻ anions connects U1 atoms to build another 1D ribbon-like chain (chain1) extend in the [010] with a bindingless U1 coordination site (Fig. 2a). And the $\left\{[(\text{UO}_2)_2\text{ipa}_2]\right\}$ dimeric motif as the unique repeating units (Fig. 2c) is found in two types of chains but with different arrangement mode (Fig. 2a,2b). The two types of chains with the included angle of 60° are further connected by U1–O12 bonds into 3D $\left\{\left\{[(\text{UO}_2)_2(\text{H}_2\text{O})_2]\text{ipa}_2\right\} \cdot \left\{[(\text{UO}_2)_2\text{ipa}_2]\right\}\right\}$ open framework with the channels in the [001] direction through interleaved mode linking fishing net (Fig. 2d).

If the positively charged dinuclear uranyl unit $[(\text{UO}_2)_2(\text{H}_2\text{O})_2]^{4+}$ regarded as a simplified metal-symbol U² which is connected to four ipa²⁻ anions from chain2 and regard UO₂²⁺ (containing U1) as U¹ connected to four ipa²⁻ anions (three in chain1 and one containing O12 in chain2), U¹ and U² could be referred to as the 3-connected and 4-connected nodes, leading to the topology of (4²·6·12³) and (4²·12⁴) with the vertex symbols of (4·12₁₂·4·12₁₂·6·12₈) and (4·4·12₂·12₂·12₁₀·12₁₀), respectively. The two types coordination of ipa²⁻ anions are each in turn bonded to three metal-symbols with L1 connected to three U¹ and L2 connected to two U² and one U¹. L1 and L2 could be referred to as the 3-connected nodes, which typically lead to (4²·6) and (4·12²) topology with the long Schläfli notation (4·4·6) and (4·12₁₆·12₁₆), respectively. Therefore, the overall topology of the present one MOF can be described as a (3,4)-connected dinodal net topology of (4·12³)₂(4²·12⁴)(4²·6·12³)₂(4²·6)₂ with the vertex symbols of (4·12₁₆·12₁₆)₂(4·4·12₂·12₂·12₁₀·12₁₀) (4·12₁₂·4·12₁₂·6·12₈)₂(4·4·6)₂ as shown in Fig. 3.

$[(\text{UO}_2)_2(\text{OH})(\text{nip})_2] \cdot \text{H}_2\text{O} \cdot \text{Et}_3\text{NH}$ (**2**). Complexes **2** features the binuclear units $[(\text{UO}_2)_2(\text{OH})\text{L}_2]$, and the asymmetric unit consists of two uranyl cations, two 5-nitroisophthalate anions (denoted as L1 and L2 ligands, which contains O3 and O11,

respectively), one deprotonated aqua ligand, one free protonated triethylamine molecule and one unbonded water molecule (Fig. 1b). The coordination environment of U atoms and nip^{2-} ligands are similar to **1**. For **2**, uranyl oxygen atoms are at an average distance of 1.779 Å from U1 and 1.780 Å from U2, and the O=U=O bond angles are all 179.2(2)°. These values fall in the normal regions which are comparable to the values reported in literatures [10]. There are also two types of ribbon-like chains, chain1 containing U1 as Fig. 4a and chain2 containing U2 as Fig. 4b, similar to **1**. Due to the protonated triethylamine molecule in the tunnel along the [001] direction, the aqua ligands of dinuclear uranyl unit $[(\text{UO}_2)_2(\text{H}_2\text{O})_2]^{4+}$ in chain2 are deprotonated to produce $[(\text{UO}_2)_2(\text{OH})_2]^{2+}$. Further, chains1 and chains2 cross-link to 3D framework by bond U1–O11 (U1–O12 for **1**) with the crossing angle is about 60° (Fig. 4c). The guest water molecules and free protonated triethylamine molecules are fasten to two “walls” of the rhombus channels by hydrogen bonds (Table S2). And **2** have the same topology to **1** (Fig. 3).

[(UO₂)₂(OH)(aip)₂]·Et₃NH (3**)**. Complexes **3** demonstrates the similar 3D framework architecture to **1** and **2**, and its asymmetric unit contains two uranyl cations UO_2^{2+} , two 5-azylisophthalate anions (denoted as L1 containing O3 and L2 containing O12, respectively), one coordinated hydroxyl ion and one free protonated triethylamine molecule (Fig. 1c). The coordination environment of U atoms and nip^{2-} ligands are similar to **1** and **2** shown in Fig. 1c. The bond lengths (U–O) of equatorial plane, U1–O and U2–O, for **3** are 2.320(8)–2.490(8) Å and 2.320(9)–2.507(9) Å respectively and the averages are 2.383 Å and 2.395 Å. The average distances of uranyl oxygen atoms from U1 and U2 are 1.719 and 1.741 Å, and the O=U=O bond angles are 178.7(4)° and 176.5(4)°, which fall in the normal regions comparing to the values reported in literatures [3d,10]. The 3D framework similar to **1** and **2** is built by two types of ribbon-like chains, chain1 containing U1 and chain2 containing U2 (Fig. 5a and 5b), through the bond U1–O12 between chain1 and chain2 with the crossing angle is 60° (Fig. 5c). The free protonated triethylamine molecules are filled to the channels, stabilized by hydrogen bonds (Table S3). **3** exhibits a (3,4)-connected dinodal net topology identical to **1** and **2** (Fig. 3).

[(UO₂)(hip)₂]·17H₂O (4**)**. Compound **4** crystallizes in the monoclinic space group *C2/c* and the structure is shown in Fig. 1d. The coordination environment of UO_2^{2+} is similar to U1 in the former three complexes, coordinated by two oxygens (O4^{#1} and O5^{#1}) from the chelating carboxyl, two oxygens (O6^{#2} and O7^{#3}) of bridging carboxyl from the different hip^{2-} and one oxygen atom of hydroxyl from the other hip^{2-} to complete a pentagonal bipyramidal chromophore. The uranyl oxygen atoms (O1 and O2) are at an average distance of 1.762 Å from U and the O=U=O bond angle is 179.7(6)°, while the average bond length (U–O) of equatorial plane is 2.369 Å, which is similar to the value of uranyl compounds [3d,10]. The two carboxylates of $\mu_4\eta^5$ nip^{2-} display two types of coordination, bidentate chelating one uranyl unit and bridging two uranyl units to form 1D chains (Fig. 6a) along two directions [110] and [10 $\bar{1}$] respectively. And the hydroxyl coordinates with the other uranyl unit by the U–O3 bond which connects two chains in different directions to build

the 3D frameworks (Fig. 6b). Comparing with complexes **1–3** constructed by two types of chains, **4** consists only a type of 1D chain similar to chain1. The lattice water molecules, which reside in cavities of the 3D framework, afford receptor for hydroxyl to form hydrogen bonds (Table S4).

Different from the acid ligands of **1–3**, the hip^{2-} ligand connected to four uranyl units is considered as four-connected nodes, and the topology is $(4^3\cdot6^2\cdot8)$ with the vertex symbols of $(4\cdot4\cdot4\cdot8_2\cdot6\cdot6)$. While the UO_2^{2+} connected to four ipa^{2-} anions (three connected by carboxyl in the same chain and one connected by hydroxy in the other chain) could be referred to as 4-connected nodes, leading to the same topology of $(4^3\cdot6^2\cdot8)$ and the same vertex symbols of $(4\cdot4\cdot4\cdot8_2\cdot6\cdot6)$. Therefore, the overall topology of the MOF can be described as a known (4,4)-connected net “*umc*” topology of $(4^3\cdot6^2\cdot8)$ with the vertex symbols of $(4\cdot4\cdot4\cdot8\cdot8\cdot10_2)$ as shown in Fig. 6c [11].

Effect of different substituent group of 5-X-1,3-dicarboxylate ligands on assembly

As is shown in the descriptions above, four uranyl MOFs with different functional group on 5-X-1,3-dicarboxylate (X = –H, –NO₂, –NH₂, –OH) were successfully synthesized and characterized. The synthesis of compounds **1–4** are summarized in scheme 3. Based on the X-ray analysis results, **1–3** feature a similar 3D architecture in which two types of chains, chain1 and chain2, exist. And the $[(\text{UO}_2)_2\text{L}_2]$ building motif is coordinated by U–O_{carboxyl} to form chain1, $[(\text{UO}_2)_2\text{L}_2]$, while bridged by two aqua ligands for **1** or hydroxide ion for **2–3** to form the similar chain2, $[(\text{UO}_2)_2(\text{H}_2\text{O})_2\text{L}_2]$. Due to the existing of organic base molecules in the 3D framework for **2–3**, the bridging block is hydroxide ion different from the aqua ligands for **1** [12]. Chain1 and chain2 are connected by uranium atom from chain1 and the carboxylic oxygen atom from chain2 to build one MOF with a topology of $(4\cdot12^2)_2(4^2\cdot12^4)(4^2\cdot6\cdot12^3)_2(4^2\cdot6)_2$. For the MOF of **4**, only one type of chain1 $[(\text{UO}_2)_2\text{L}_2]$ exist, which is further coordinated by U atom from one chain and O atom of –OH from another chain to intersect one MOF with a “*umc*” topology of $(4^3\cdot6^2\cdot8)$.

Compounds **1–3** (X = –H for **1**, –NO₂ for **2**, –NH₂ for **3**) possess similar 3D framework but different guest filling molecules. For **1** (X = –H), no free guest molecule fill in the channel. For **2** (X = –NO₂), the free water and triethylamine molecules are fill in the framework by the rich hydrogen bonds. While for **3** (X = –NH₂), only the guest triethylamine molecules reside in the cavities of repeated rhomboids. Due the strong coordination ability of –OH, complex **4** (X = –OH) exhibits the different 3D architecture from **1–3**, and the water molecules reside in the channels stabilized by the hydrogen bonds.

For investigate the complexes based 5-X-1,3-dicarboxylate ligands systematically, all the relevant reported compounds are summarized in table 2. When the 5-X-1,3-benzenedicarboxylic acid adopts $\mu_3\eta^4$ coordination (type a in scheme 2), the 7-fold coordinated uranium atom is always found in the uranyl complexes possessing the same 14-membered ring structural motif (type A in table 2), “ $[(\text{UO}_2)_2\text{L}_2]$ ”. While the two carboxyls

of 5-X-1,3-benzenedicarboxylic acid all adopt chelating way, the 8-fold coordinated uranium atom is found in the only two reported compounds, in which exist another motif (type B in table 2), “[UO₂L₃]”.

Optical band gaps

The UV/Vis absorption spectra measured for powder of compounds **2** and **4** are shown in Fig. S1. To determine the band gap energy (E_g) of the obtained complex, the Kubelka–Munk method based on the diffuse reflectance spectra was employed. The gap energies were determined from a plot of $(F(R)hv)^{0.5}$ versus photon energy (hv), where $F(R) = (1-R)^2/2R$ [17], where h –Planck constant, m –frequency of electromagnetic wave, and R –reflectance.

As illustrated in Fig. 7, the E_g value assessed from the steep absorption edge of compounds **2** is 2.12 eV, while the E_g values, 2.20 could be found for compound **4**. The values of the above two complexes corresponds to the characteristic value of uranyl compounds about the forbidden band [1b,18]. This confirms that the complexes can be activated by radiation from ultraviolet and by visible light regions. Therefore, the photocatalytic activities for **2** and **4** are measured.

Luminescent properties

The emission spectra under excitation at the wavelength of 420 nm for the bulk products of compound **1** and compound **2**, 370 nm for the bulk products of compound **3** and 240 nm for compound **4** were recorded in the solid state (Fig. 8). As the visible fluorescence property of ipa ligand, compound **1** exhibits two extremely strong emission peaks at 529 and 545 nm, which can be seen as two significantly characteristic peaks of uranyl complexes. The above phenomenon is assigned to ligand to metal charge transfer (LMCT) to strengthen the emission intensity of uranyl cation. Five prominent peaks, 481, 498, 519, 542, 567 nm, are clearly observed for compound **2**, corresponding to the electronic and vibronic transitions $S_{11}-S_{00}$ and $S_{10}-S_{0v}$ ($v = 0-4$). Such a spectrum is typical for most uranyl compounds, which exhibit green light centered near 520 nm and often consist of several peaks [19], and this is a charge-transfer-based emission that is vibrationally coupled to both bending and stretching modes of the uranyl cation [20]. Compared to a benchmark compound UO₂Ac₂·2H₂O (max at 511 nm) [21], the luminescence spectrum of **2** exhibits a slight red shift by a value of 8 nm. For compound **3**, the absence of strong emission lines in the spectrum shows a broad peak with three weak and poorly resolved uranyl emissions, 391, 408, 429 nm, which may be caused by the impact of the emission of aip ligand. While for **4**, only shows two broad emissions of the coordinated hip ligand but no classic emissions of uranyl cation are observed. This is a common phenomenon because not all uranyl compounds exhibit luminescent properties due to their interior nature in bonding [22], size, and quality of the crystals [20], etc. On the basis of these spectra, the impact of the different substituent groups in the acid ligand on the luminescent properties of the complexes is obvious.

Photocatalytic activities

Photocatalysts have attracted much attention due to their potential applications in purifying water and air by decomposing organic molecules [23]. To our knowledge, TiO₂ has been studied extensively as a semiconductor photocatalyst. However, a main drawback for its application in wastewater treatment is its broad forbidden band (3.0~3.2 eV) [24]. And the nanoscale TiO₂ can only use part of the UV light of the sunlight. Thus, the photocatalysts of uranyl-organic coordination polymers and frameworks (UOFs) which can use sunlight have attracted much attention [21,25]. RhB, as a model dye contaminant, was selected to evaluate photocatalytic effectiveness in the purification of wastewater. Moreover, the title complexes are water-insoluble photocatalyst. Thus, the photocatalytic activity of as-prepared **2** and **4** was tested by the degradation of RhB solution under simulate daylight irradiation of xenon lamp, being a model reaction. For comparison, the photodegradation process of RhB without any photocatalyst has also been studied under the same conditions.

It can be seen in Fig. 9c that the concentrations of RhB without any photocatalyst is almost no changed and the photocatalytic activities increase to 94% for **2** and 78% for **4** after 160 min of irradiation of 500 W xenon lamp. Obviously, the degradation efficiency of **2** under simulate daylight is higher than **4**. In ref 21, under the irradiation of the mercury lamp, the concentration of the RhB solution is 10.0 mg·L⁻¹ and the ratio of weight of photocatalyst and volume of the solution is 0.5 mg·mL⁻¹. Compared with the above uranyl photocatalysts, we used the xenon lamp to simulate nature light and RhB solution with higher concentration (30.0 mg·L⁻¹). The complexes in ref 20 need 130~160 min of irradiation to degrade about all the target dye, which shows that the photocatalytic activity for the two photocatalysts is superior to some complexes reported [21]. The results indicate that the two complexes show activities and stabilities in the degradation of RhB under simulate daylight irradiation of xenon lamp.

For investigate the impact of the illumination intensity and power of the xenon lamp to the photodegradation efficiency, the photodegradation tests of photocatalyst **2** upon irradiation in 700 W and 300 W are also measured. As showed in Fig. 10, the degradation rate of RhB is obviously different upon irradiation of three xenon lamp with different power. The RhB is degraded incompletely upon 300 W at 160 min, while is degraded about 95% upon 700 W only at 120 min. The above result explains that the illumination intensity and power of the Xenon lamp would influence the photodegradation rate.

Comparing uranyl ion (UO₂²⁺) to conventional TiO₂ photocatalyst, UO₂²⁺ is unique as it responds more quickly and has a higher-efficiency not only because of its fairly strong absorption upon sunlight irradiation, but also because of its particular photocatalytic mechanism characterized by a distinct process of hydrogen abstraction and electron transfer [26-28]. The particular properties of uranyl based compounds principally depend on their unique electronic and geometric structure, the axial uranium–oxygen bonds are short, strong, and collinear. The

uranyl ion possesses a long-lived and highly oxidizing excited state owing to a $U_{5f} \leftarrow O_{2p}$ ligand-to-metal charge transfer (LMCT) with the UO_2^{2+} group. The highest occupied molecular orbitals (HOMO) forms as a result of interaction of the U_{5f} orbitals with the symmetry match O_{2p} group orbitals. However, the lowest unoccupied molecular orbitals (LUMO) are nonbonding orbitals localized on the uranium atom. The LMCT excitations of electrons from the highest occupied and ligand-based bonding orbitals to the nonbonding U_{5f} orbitals are responsible for the formation of oxygen-centered radical. While the nucleophilic group of organic molecules (such as RhB) with an appropriate orientation are within a reasonable range, electrons from these molecules may be abstracted by the excited $^*UO_2^{2+}$ species, resulting in intermediates and protons. As the electrons from the guest molecules occupy the HOMO, the excited electrons in the uranyl unit would remain in the LUMO. However, electronegative substances, such as O_2 in the solution would capture the excited electrons in the uranyl unit to generate highly active peroxide anions. The produced organic intermediates in the solution are further oxidized and decomposed by the strong oxidizing peroxide anions, completing the degradation of the organic substances. As a result, the entire processes of photochemical reactions can be related to a variety of factors such as the electron structure of the uranyl species, the electronic transition of the ground state to the excited state, charge transfer between uranyl species and organic molecules, the proton abstraction, the formation of a radical and the absorption of the substrate, and so on.

Conclusions

Four new 3D uranyl compounds were hydrothermally synthesized and display structural relevance as a function of the variation about substituent groups of the title acid ligands, 5-X-1,3-benzenedicarboxylic acid ($X = -H, -NO_2, -NH_2, -OH$), which was selected in an effort to explore the influence of traditional metal–ligand coordination on uranyl hybrid material assembly. The four compounds presented a dinuclear motif, $[(UO_2)_2L_2]$, which gave rise to two type of chains. In compound 1–3, direct coordination through U–O (O from carboxyl) bonds between two types of chains gave rise a 3D framework. While compound 4 is built by the U–O (O from hydroxyl on hip ligand) bonds between the each other chains. The different substituent groups generate two types of 3D framework and result in the different of guest molecules. Additionally, the great difference of fluorescence spectra for these compounds illustrates the significant impact of the different substituent groups on the properties of the complexes. As the prominent property of uranyl compounds, the photocatalytic activities for compound 2 and 4 are measured and the two compounds can degrade RhB (30 mg/L) to 94% for 2 and 78% for 4 after 160 min of solar simulator irradiation with 1 mg/mL photocatalyst, which exhibits the above two compounds may be good and stable photocatalyst for the photodegradation of RhB under daylight irradiation, but shows no photocatalytic activity for azo dyes such as methyl orange, acid orange. And our efforts are now continuously dedicated to

utilization of the analogous isophthalic acid ligands with different substituent groups such as halogenated acid to explore the new uranyl-organic photocatalyst which can degrade the most dyestuff containing azo dyes.

Acknowledgement

This project was supported by Education Department of Zhejiang Province and the K.C. Wong Magna Fund in Ningbo University.

Notes and references

Crystal Engineering Division, Center for Applied Solid State Chemistry Research, Ningbo University, Ningbo, 315211, P.R. China. Fax: +574/87600747; Tel: +574/87600747; E-mail: zhengcm@nbu.edu.cn

† Electronic Supplementary Information (ESI) available: [Selected interatomic distances and bond angles table, PXRD patterns with the simulated patterns from the single crystal structure data for 2 and 4, Infrared spectra for 2 and 4, and UV-Vis solid state reflectance spectra for 2 and 4. CCDC reference numbers 1024949–1024952]. For ESI and crystallographic data cif or their electronic format see DOI: xx.xxxx/xxxxxxxxx/

- (a) P. A. Giesting, P. C. Burns, *Cryst. Rev.*, 2006, **12**, 205. (b) W. T. Yang, H. Y. Wu, R. X. Wang, Q. J. Pan, Z. M. Sun, H. J. Zhang, *Inorg. Chem.*, 2012, **51**, 11458. (c) M. B. Andrews, C. L. Cahill, *Chem. Rev.*, 2013, **113**, 1121. (d) T. Loiseau, I. Mihalcea, N. Henry, *Coord. Chem. Rev.*, 2014, **266–267**, 69. (e) T. Tian, W. T. Yang, H. Wang, S. Dang, Q. J. Pan, Z. M. Sun, *Inorg. Chem.*, 2013, **52**, 7100.
- P. A. Giesting, P. C. Burns, *Crystallogr. Rev.*, 2006, **12**, 205.
- (a) A. Kirishima, T. Kimura, O. Tochiyama, Z. Yoshida, *J. Alloys Compd.*, 2004, **374**, 277. (b) C. E. Rowland, C. L. Cahill, *Inorg. Chem.*, 2010, **49**, 8668. (c) K. E. Knope, L. Soderholm, *Chem. Rev.*, 2013, **113**, 944. (d) I. Mihalcea, N. Henry, C. Volkringer, T. Loiseau, *Cryst. Growth Des.*, 2012, **12**, 526. (e) T. Tian, W. T. Yang, H. Wang, S. Dang, Z. M. Sun, *Inorg. Chem.*, 2013, **52**, 8288.
- (a) J. Leciejewicz, N. Alcock, T. Kemp, *J. Coord. Chem.*, 1995, **82**, 43. (b) H. Y. Wu, R. X. Wang, W. Yang, J. Chen, Z. M. Sun, J. Li, H. Zhang, *Inorg. Chem.*, 2012, **51**, 3103. (c) I. Mihalcea, C. Volkringer, N. Henry, T. Loiseau, *Inorg. Chem.*, 2012, **51**, 9610. (d) R. C. Severance, S. A. Vaughn, M. D. Smith, H. C. zur Loye, *Solid State Sci.*, 2011, **13**, 1344. (e) P. Thuéry, *Cryst. Growth Des.*, 2011, **11**, 2606.
- L. Carlucci, G. Ciani, D. M. Proserpio, A. Sironi, *Angew. Chem. Int. Ed. Engl.*, 1995, **34**, 1895.
- (a) S. G. Murry, E. R. Hartley, *Chem. Rev.*, 1981, **81**, 365. (b) X. H. Bu, W. Chela, S. L. Lu, H. Zhang, D. Z. Liao, W. M. Bu, M. Shionoya, F. Brisse, J. Ribas, *Angew. Chem. Int. Ed.*, 2001, **40**, 3201. (c) M. A. Withersby, A. J. Blake, N. R. Champness, P. A. Cooke, P. Hubberstey, W. S. Li, M. Schrolder, *Inorg. Chem.*, 1999, **38**, 2259. (d) Y. J. Kim; E. W. Lee; D. Y. Jung, *Chem. Mater.*, 2001, **13**, 2684.
- (a) C. Volkringer, I. Mihalcea, J. F. Vigier, A. Beaurain, M. Visseaux, T. Loiseau, *Inorg. Chem.*, 2011, **50**, 11865. (b) L. A. Borkowski, C. L. Cahill, *Acta Cryst.*, 2004, **E60**, m198.
- (a) G. M. Sheldrick, SHELXS-97, Programm zur Lösung von Kristallstrukturen, Göttingen, 1997. (b) G. M. Sheldrick, SHELXL-97, Programm zur Verfeinerung von Kristallstrukturen, Göttingen, 1997.
- A. L. J. Spek, *Appl. Crystallogr.*, 2003, **36**, 7.
- (a) Y. Xia, K. X. Wang, J. S. Chen, *Inorg. Chem. Commun.*, 2010, **13**, 1542. (b) I. Mihalcea, N. Henry, T. Bousquet, C. Volkringer, T. Loiseau, *Cryst. Growth Des.*, 2012, **12**, 4641. (c) A. Bismondoa, U. Casellato, R. Graziani, *Inorg. Chim. Acta*, 1994, **223**, 151.
- T. T. Lian, S. M. Chen, A new Mn(II) coordination polymer with 4-connected *umc* topology and luminescent property, The sixth Chinese chemical society national structural chemistry seminars, 2012.

- 12 (a) B. Masci, P. Thuéry, *Polyhedron*, 2005, **24**, 229. (b) P. Thuéry, *Inorg. Chem. Commun.*, 2008, **11**, 616. (c) W. Yang, T. Tian, H. Y. Wu, Q. J. Pan, S. Dang, Z. M. Sun, *Inorg. Chem.*, 2013, **52**, 2736. (d) M. Mirzaei, H. Eshtiagh-Hosseini, V. Lippolis, H. Aghabozorg, D. Kordestani, A. Shokrollahi, R. Aghaei, A. J. Blake, *Inorg. Chim. Acta*, 2011, **370**, 141.
- 13 J. Y. Kim, A. J. Norquist, D. O'Hare, *Dalton Trans.*, 2003, 2813.
- 14 I. Mihalcea, N. Henry, N. Clavier, N. Dacheux, T. Loiseau, *Inorg. Chem.*, 2011, **50**, 6243.
- 10 15 P. Thuéry, *CrystEngComm*, 2013, **15**, 2401.
- 16 P. M. Cantos, C. L. Cahill, *Cryst. Growth Des.*, 2014, **14**, 3044.
- 17 A. B. Murphy, *Sol. Energ. Mat. Sol. C*, 2007, **91**, 1326.
- 18 X. S. Zhai, Y. Q. Zheng, J. L. Lin, W. Xu, *Inorg. Chim. Acta*, 2014, **423**, 1.
- 15 19 (a) A. T. Kerr, C. L. Cahill, *Cryst. Growth Des.*, 2014, **14**, 1914. (b) P. Thuéry, J. Harrowfield, *Cryst. Growth Des.*, 2014, **14**, 1314. (c) H. Y. Wu, W. Yang, Z. M. Sun, *Cryst. Growth Des.*, 2012, **12**, 4669.
- 20 G. Liu, J. V. Beitz, *The Chemistry of the Actinide and Transactinide Elements*; L. R. Morss, N. M. Edelstein, J. Fuger, Eds. Springer: Heidelberg, 2006.
- 21 Y. N. Hou, Y. H. Xing, F. Y. Bai, Q. L. Guan, X. Wang, R. Zhang, Z. Shi, *Spectrochim. Acta A*, 2014, **123**, 267.
- 22 P. O. Adelani, T. E. Albrecht-Schmitt, *Cryst. Growth Des.*, 2011, **11**, 4227.
- 25 23 (a) M. R. Hoffmann, S. T. Martin, W. Choi, D. W. Bahnemann, *Chem. Rev.*, 1995, **95**, 69. (b) K. Pirkanniemi, M. Sillanpää, *Chemosphere*, 2002, **48**, 1047.
- 24 A. Fujishima, K. Honda, *Nature*, 1972, **238**, 37.
- 25 (a) Z. T. Yu, Z. L. Liao, Y. S. Jiang, G. H. Li, G. D. Li, J. S. Chen, *Chem. Commun.*, 2004, 1814. (b) Z. T. Yu, Z. L. Liao, Y. S. Jiang, G. H. Li, J. S. Chen, *Chem. Eur. J.*, 2005, **11**, 2642. (c) Z. L. Liao, G. D. Li, M. H. Bi, J. S. Chen, *Inorg. Chem.*, 2008, **47**, 4844. (d) W. T. Yang, W. G. Tian, X. X. Liu, L. Wang, Z. M. Sun, *Cryst. Growth Des.*, 2014, **14**, 5904. (e) W. T. Yang, H. Wang, W. G. Tian, J. Y. Li, Z. M. Sun, *Eur. J. Inorg. Chem.*, 2014, 5378.
- 35 26 (a) V. A. Volkovich, T. R. Griffiths, D. J. Fray, R. C. Thied, *Phys. Chem. Chem. Phys.*, 2001, **3**, 5182. (b) R. G. Denning, *J. Phys. Chem. A*, 2007, **111**, 4125.
- 27 K. X. Wang, J. S. Chen, *Acc. Chem. Res.*, 2011, **44**, 531.
- 40 28 (a) Y. Li, J. Su, E. Mitchell, G. Q. Zhang, J. Li, *Sci. China Chem.*, 2013, **56**, 1671. (b) H. D. Burrows, T. J. Kemp, *Chem. Soc. Rev.*, 1974, 139.

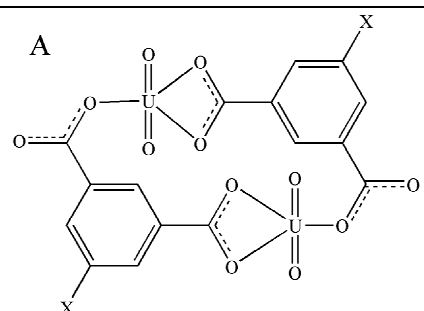
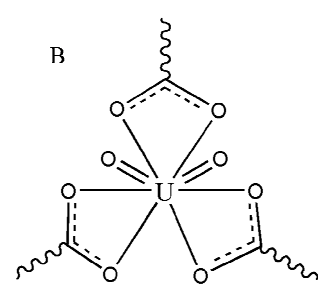
Table 1. Summary of crystal data collection, structure solution and refinement detail for 1–4 ($T = 293(2)$)

Compounds	1	2	3	4
Empirical formula	$C_{16}H_{28}O_{22}U_2$	$C_{22}H_{26}N_3O_{18}U_2$	$C_{22}H_{28}N_3O_{13}U_2$	$C_{16}H_{42}O_{31}U_2$
Formula weight	1048.30	1096.52	1018.53	1206.30
Crystal system	triclinic	triclinic	triclinic	monoclinic
Description	yellow, block	yellow, block	yellow, block	orange, block
Crystal size/mm	$0.18 \times 0.16 \times 0.15$	$0.35 \times 0.12 \times 0.11$	$0.30 \times 0.18 \times 0.15$	$0.38 \times 0.36 \times 0.35$
Space group	$P\bar{1}$	$P\bar{1}$	$P\bar{1}$	$C2/c$
$a/\text{\AA}$	9.666(2)	10.663(2)	9.642(2)	19.703(4)
$b/\text{\AA}$	11.002(2)	11.090(2)	10.973(2)	9.520(2)
$c/\text{\AA}$	15.304(3)	14.718(3)	15.997(3)	20.127(4)
α°	108.95(3)	106.88(3)	109.52(3)	90
β°	95.14(3)	95.76(3)	91.56(3)	106.26(3)
γ°	109.32(3)	112.99(3)	109.61(3)	90
Volume/ \AA^3	1416.7(7)	1487.4(8)	1484.0(7)	3624.2(14)
Z	2	2	2	4
$D_c/\text{g}\cdot\text{cm}^{-3}$	2.457	2.446	2.277	2.211
$F(000)$	788	1012	936	1640
μ/mm^{-1}	11.465	10.960	10.964	8.971
θ Range/ $^\circ$	2.99–25.00	3.01–27.48	3.02–27.48	2.99–27.44
Reflections collected	11274	14774	14242	16567
Unique reflections (R_{int})	4999 ($R_{\text{int}} = 0.0639$)	6828 ($R_{\text{int}} = 0.0928$)	6699 ($R_{\text{int}} = 0.1198$)	4152 ($R_{\text{int}} = 0.0583$)
Data, restraints, parameters	3778, 189, 288	5827, 4, 412	3943, 432, 417	3038, 13, 153
Goodness of fit on F^2	1.116	1.067	1.021	1.152
$R_1, wR_2 [I \geq 2\sigma(I)]^a$	0.0521, 0.1405	0.0379, 0.0934	0.0761, 0.1603	0.0576, 0.0874
R_1, wR_2 (all data) ^a	0.0775, 0.1778	0.0461, 0.0988	0.1189, 0.1980	0.1451, 0.1917
A, B values in w^b	0.0862, 15.2636	0.0365, 2.1101	0.0500, 18.0000	0.0756, 160.8163
$\delta\rho_{\text{max}}, \delta\rho_{\text{min}}$ ($e\cdot\text{\AA}^{-3}$)	2.528, -3.378	4.278, -3.588	4.049, -3.583	2.533, -4.074

$$^a) R_1 = \frac{\sum(|F_o| - |F_c|)}{\sum|F_o|}, wR_2 = \left[\frac{\sum w(F_o^2 - F_c^2)^2}{\sum w(F_o^2)^2} \right]^{1/2}$$

$$^b) w = [\sigma^2(F_o^2) + (AP)^2 + BP]^{-1} \text{ with } P = (F_o^2 + 2F_c^2)/3$$

Table 2. Summary of the relevant compounds reported based 5-X-1,3-dicarboxylate ligands

Type	Compounds	Space group	Dimensionality	Coordination of U	Structural feature
a	$[\text{UO}_2(\text{tma})(\text{H}_2\text{O})] \cdot \text{H}_2\text{O}$ ^[7b]	$P\bar{1}$	1D	7-fold coordination	
	$[\text{UO}_2(\text{sip})] \cdot \text{HTEA}$ ^[12c,15]	$P\bar{1}$	2D	7-fold coordination	
	$[\text{UO}_2(\text{sip})] \cdot \text{HPYZ} \cdot 2.5\text{H}_2\text{O}$ ^[15]	$P2_1/c$	2D	7-fold coordination	
	$[(\text{UO}_2)_2(\text{OH})(\text{O})(\text{sip})] \cdot 2\text{HDIB}$ ^[16]	$P2_1/n$	2D	7-fold coordination	
	$[(\text{UO}_2)(\text{nip})(\text{H}_2\text{O})] \cdot \text{H}_2\text{O}$ ^[16]	$P\bar{1}$	1D	7-fold coordination	
	$[(\text{UO}_2)_2(\text{nip})_2\text{H}_2\text{O}] \cdot \text{TEA}$ ^[16]	$P\bar{1}$	2D	7-fold coordination	
	$[(\text{UO}_2)_2(\text{H}_2\text{O})(\text{aip})_2] \cdot \text{TEA}$ ^[this work]	$P\bar{1}$	3D	7-fold coordination	
	$[(\text{UO}_2)_2(\text{H}_2\text{O})(\text{ipa})_2]$ ^[this work]	$P\bar{1}$	3D	7-fold coordination	
	$[(\text{UO}_2)_2(\text{H}_2\text{O})(\text{nip})_2] \cdot \text{TEA} \cdot \text{H}_2\text{O}$ ^[this work]	$P\bar{1}$	3D	7-fold coordination	
	$[(\text{UO}_2)(\text{hip})]_2 \cdot \text{H}_2\text{O}$ ^[this work]	$C2/c$	3D	7-fold coordination	
b	$(\text{UO}_2)_8\text{O}_2(\text{OH})_4(\text{H}_2\text{O})_4(\text{ipa})_4 \cdot 4\text{H}_2\text{O}$ ^[16]	$P\bar{1}$	3D	7-fold coordination	—
	$\text{UO}_2(\text{ipa})$ ^[10b]	$C2/c$	3D	6-fold coordination	—
c	$[(\text{UO}_2)_{1.5}(\text{ipa})_2]_2[\text{CH}_3\text{NCOH}_2] \cdot \text{H}_2\text{O}$ ^[13]	$P2_1/n$	1D	8-fold coordination	
	$[\text{Ni}_2(\text{bipym})_3(\text{H}_2\text{O})_4][\text{UO}_2(\text{sip})(\text{NO}_3)]_2 \cdot 6\text{H}_2\text{O}$ ^[13]	$P\bar{1}$	1D	8-fold coordination	
d	$[\text{UO}_2(\text{sip})(\text{H}_2\text{O})]_2 \cdot \text{H}_2\text{DABCO} \cdot 4\text{H}_2\text{O}$ ^[15]	$P2_1/c$	3D	7-fold coordination	—
	$[(\text{UO}_2)(\text{nip})(\text{Hnip})] \cdot \text{HTMA}$ ^[16]	$P2_1/c$	1D	7-fold coordination	—

Note: tma = 1,3,5-tricarboxylic acid, sip = 5-sulfoisophthalic acid, ipa = isophthalic acid, nip = 5-nitroisophthalic acid, aip = 5-aminoisophthalic acid, hip = 5-hydroxyisophthalic acid, TEA = triethylamine, PYZ = pyrazine, DIB = 1,4-di(1Himidazol-1-yl)benzene, bipym = 2,2'-bipyrimidine

Scheme captions

Scheme 1. Schematic representation of 5-X-1,3-dicarboxylate ligands.

Scheme 2. The coordination modes of 5-X-1,3-dicarboxylate ligands.

Scheme 3. Schematic illustration of the synthetic processes and assembling for compounds 1–4.

Figure captions

Fig. 1 ORTEP view of coordination environment of UO_2^{2+} and the ipa^{2-} in $[(\text{UO}_2)_2(\text{H}_2\text{O})(\text{ipa})_2]$ (**1**), $[(\text{UO}_2)_2(\text{H}_2\text{O})(\text{nip})_2]\cdot\text{H}_2\text{O}\cdot\text{Et}_3\text{NH}$ (**2**), $[(\text{UO}_2)_2(\text{H}_2\text{O})(\text{aip})_2]\cdot\text{Et}_3\text{NH}$ (**3**) and $[(\text{UO}_2)(\text{hip})]_2\cdot\text{H}_2\text{O}$ (**4**) together with the atom numbering scheme corresponding to (a) to (d), respectively. Thermal ellipsoids are drawn at 30% probability level (Symmetry transformations used to generate equivalent atoms: (a) for **1**: #1 = $-x, -y-1, -z+1$; #2 = $-x+1, -y, -z+1$; #3 = $x, y-1, z$; #4 = $x, y+1, z$; #5 = $-x+2, -y+1, -z$. (b) for **2**: #1 = $-x+3, -y+3, -z+1$; #2 = $-x+2, -y+2, -z+1$; #3 = $x, y+1, z$; #4 = $x, y-1, z$; #5 = $-x+1, -y+1, -z+2$. (c) for **3**: #1 = $-x-1, -y-1, -z$; #2 = $-x-2, -y-2, -z$; #3 = $x, y+1, z$; #4 = $x, y-1, z$; #5 = $-x-3, -y-3, -z+1$. (d) for **4**: #1 = $-x+0.5, -y+0.5, -z+0.5$; #2 = $x, -y+1, z-0.5$; #3 = $-x, y, -z+0.5$; #4 = $x, -y+1, z+0.5$; #5 = $-x+0.5, y-0.5, -z+0.5$).

Fig. 2 (a) 1D ribbon-like chain1 in **1** assembly by the $\infty^1[(\text{UO}_2)_2\text{ipa}_2]$ dimeric motif with an unoccupied connector. (b) 1D chain2 in **1** assembly by the $\infty^1[(\text{UO}_2)_2\text{ipa}_2]$ dimeric motif via the bridging role of aqua ligands. (c) The cut dimeric motif $\infty^1[(\text{UO}_2)_2\text{ipa}_2]$. (d) 3D architecture built from two types of chains with the connector.

Fig. 3 Schematic view of the net topology of **1–3**.

Fig. 4 (a) 1D ribbon-like chain1 in **2** assembly by the dimeric motif. (b) 1D chain2 in **2** assembly by the dimeric motif via the bridging role of hydroxyl ions. (c) 3D architecture built from two types of chains with the connector and the guest triethylamine and water molecules fill in the channel.

Fig. 5 (a) 1D ribbon-like chain1 in **3** assembly by the dimeric motif. (b) 1D chain2 in **3** assembly by the dimeric motif via the bridging role of hydroxyl ions. (c) 3D architecture built from two types of chains with the connector and the guest triethylamine molecules fill in the channel.

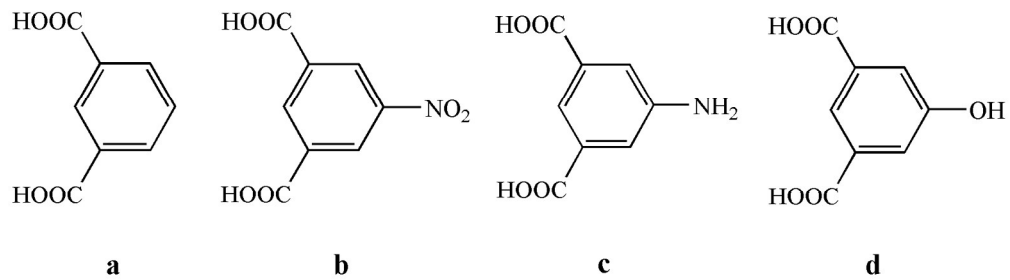
Fig. 6 (a) 1D ribbon-like chain in **4** assembly by the dimeric motif. (b) 3D architecture built from 1D chains with the connector. (c) Schematic view of the net topology of **4**.

Fig. 7 Diffuse reflectance UV-VIS-NIR spectra of K-M functions *versus* energy (eV) of compounds **2** and **4**.

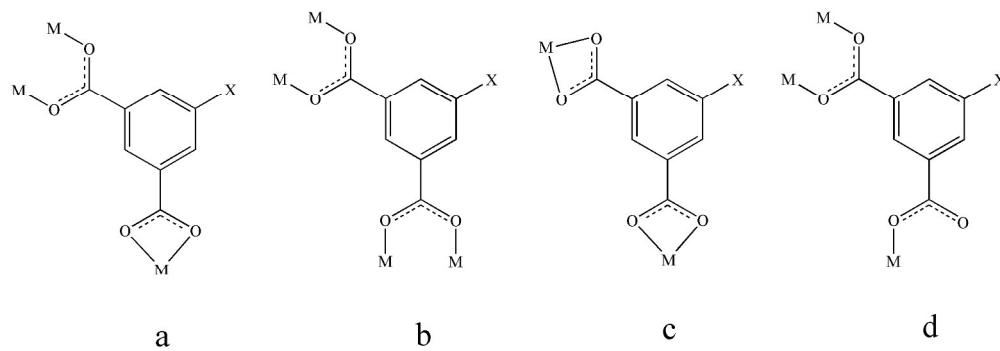
Fig. 8 Solid-state emission spectra of complexes **2** and **4** and the bulk products of compounds **1** and **3** at room temperature.

Fig. 9 (a) and (b) Absorption spectra of the RhB solution during the decomposition reaction with the use of complexes **2** and **4**. (c) Photocatalytic decomposition of RhB solution with the change in C_t/C_0 of **2** and **4**, and triangle curve is the control experiment without any catalyst.

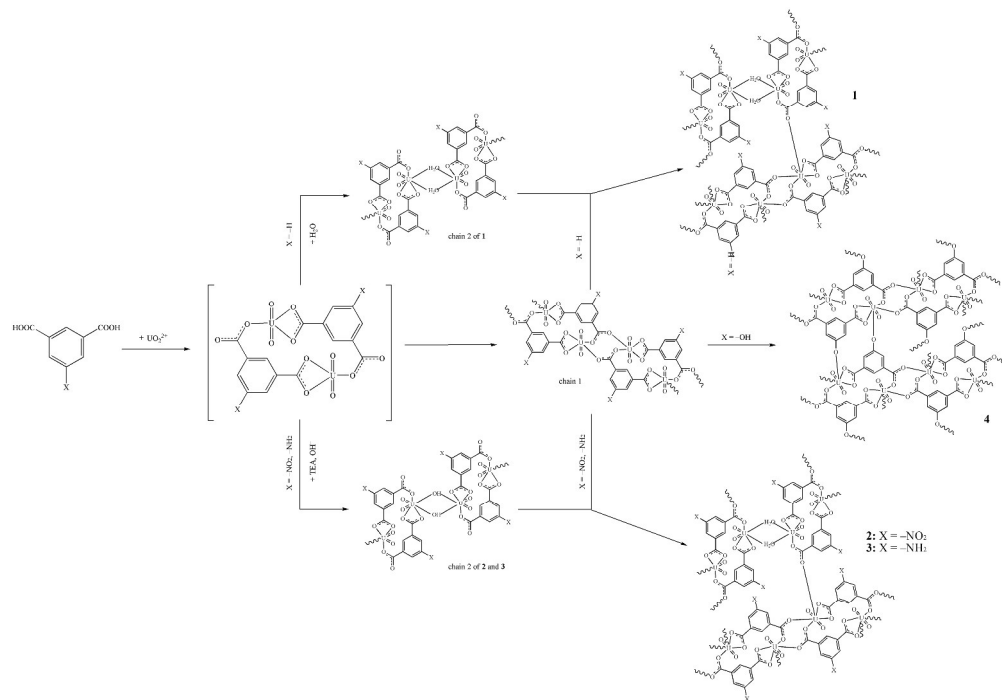
Fig. 10 Photocatalytic decomposition of RhB solution with the change in C_t/C_0 of **2** upon irradiation of three xenon lamp with three different power.



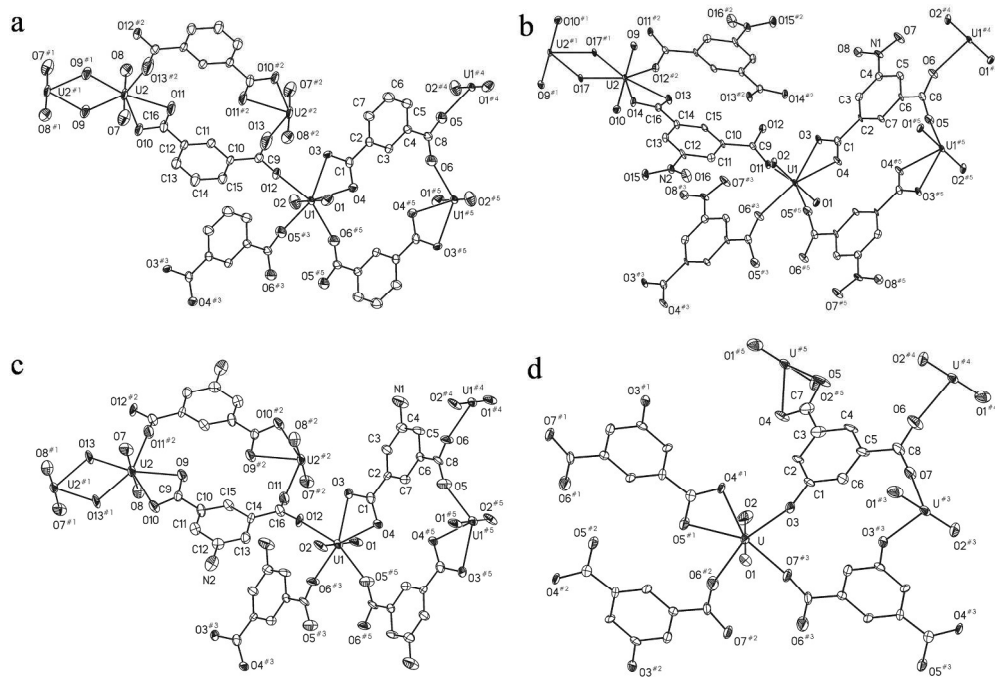
169x47mm (300 x 300 DPI)



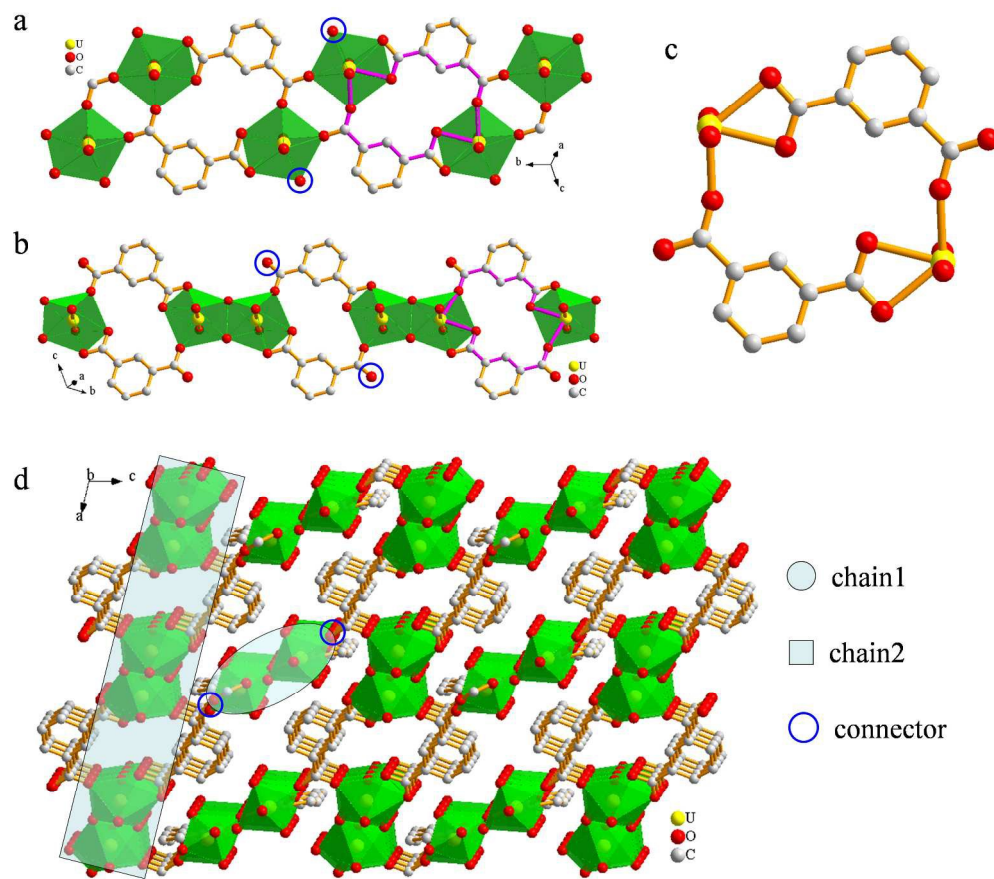
260x90mm (300 x 300 DPI)



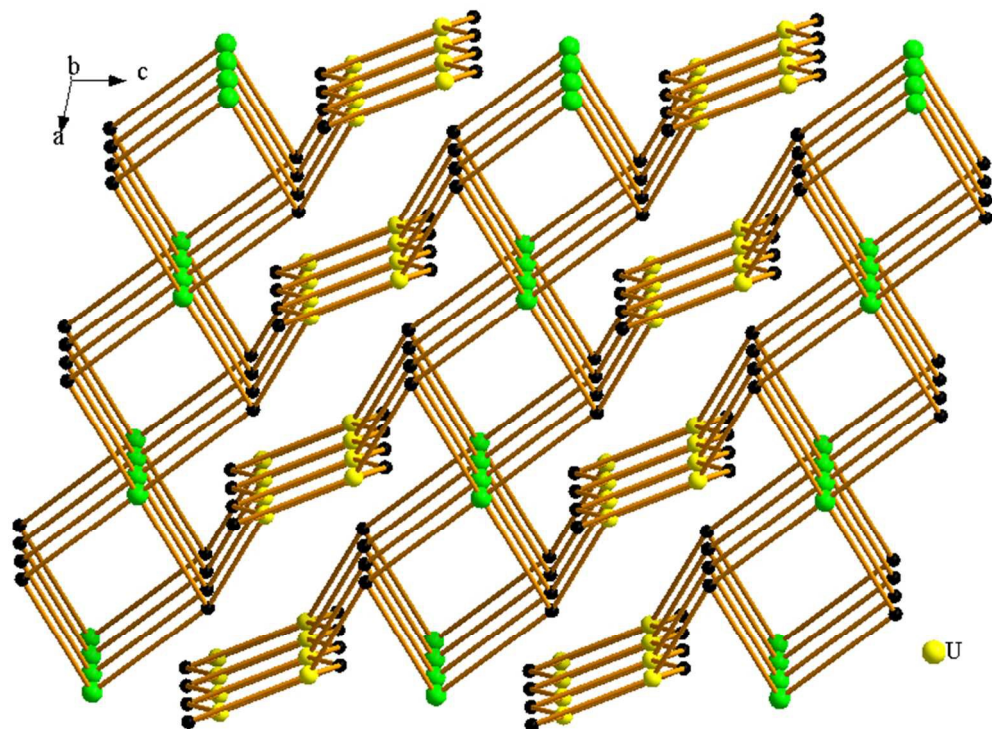
536x372mm (300 x 300 DPI)



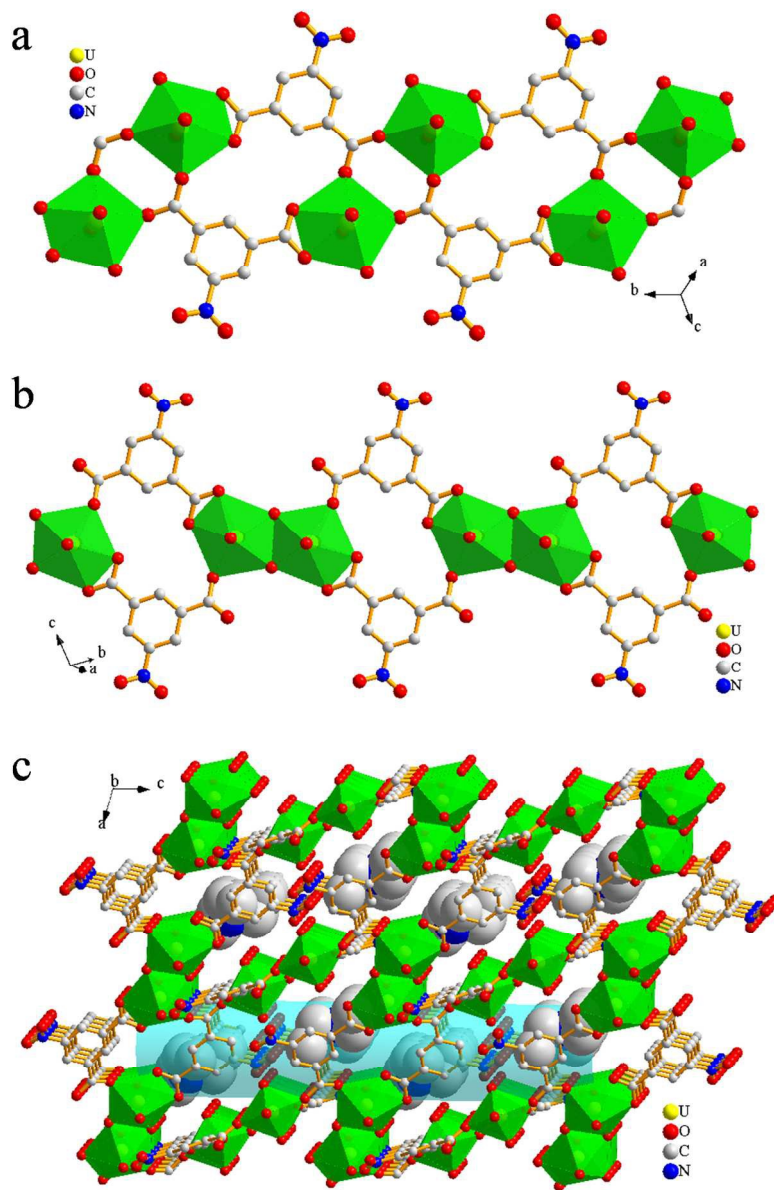
501x343mm (149 x 149 DPI)



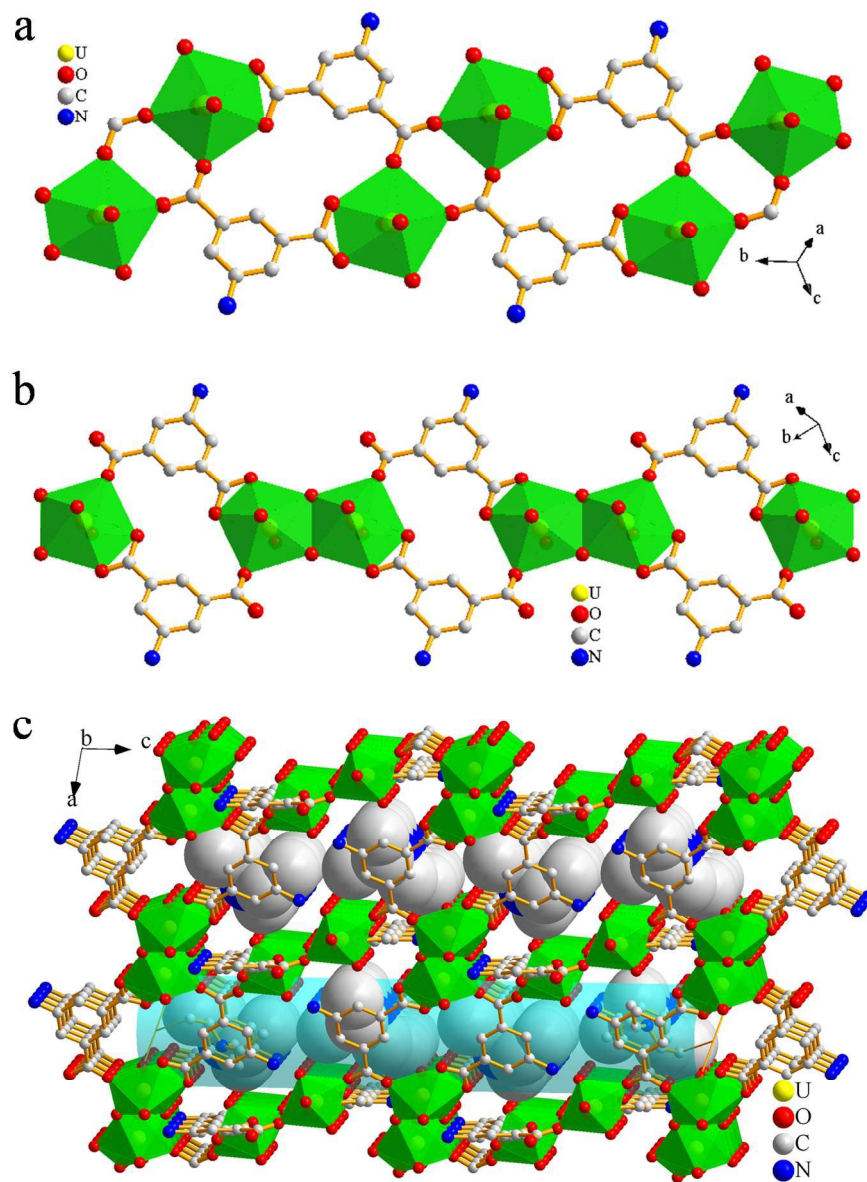
445x392mm (150 x 150 DPI)



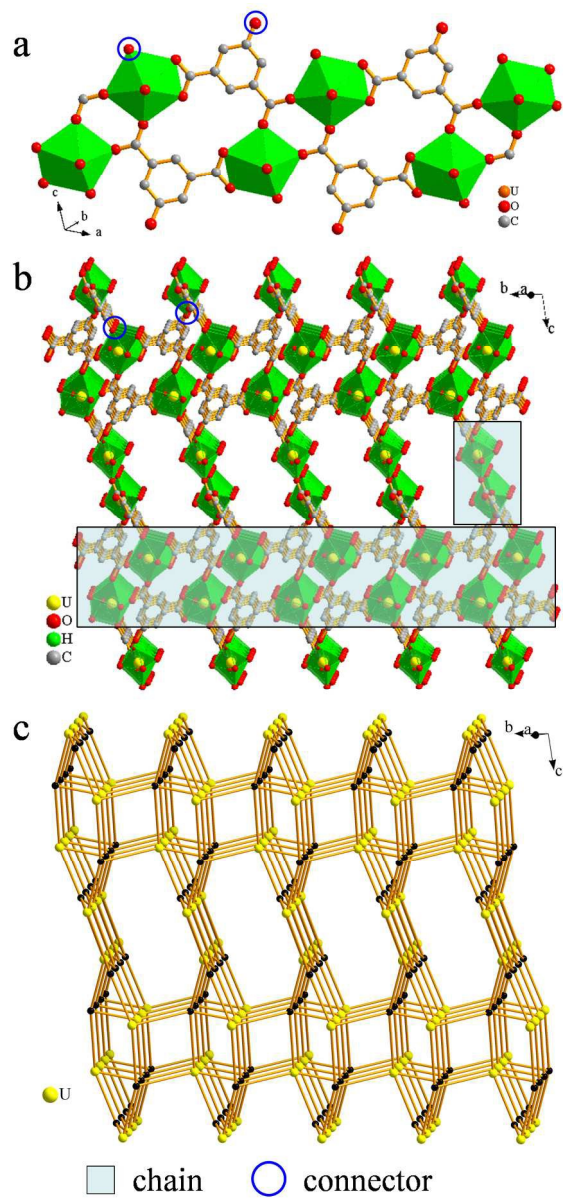
207x152mm (96 x 96 DPI)



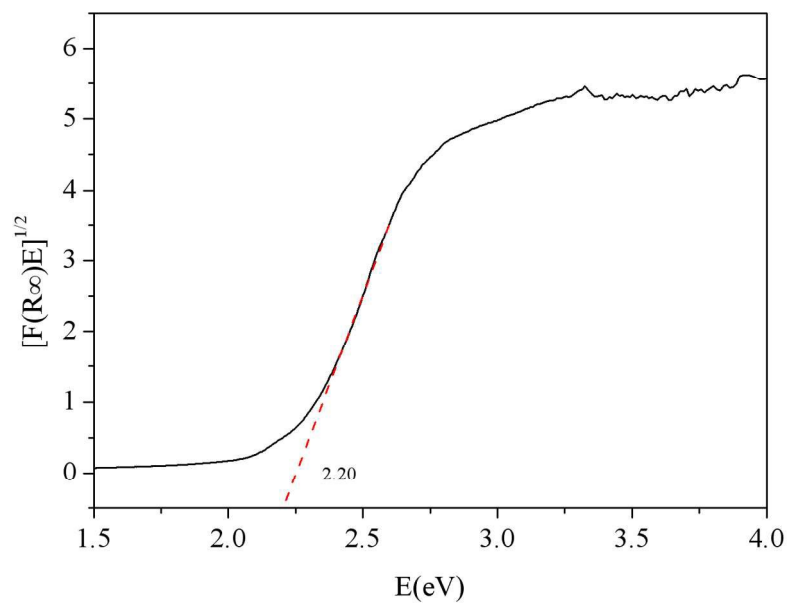
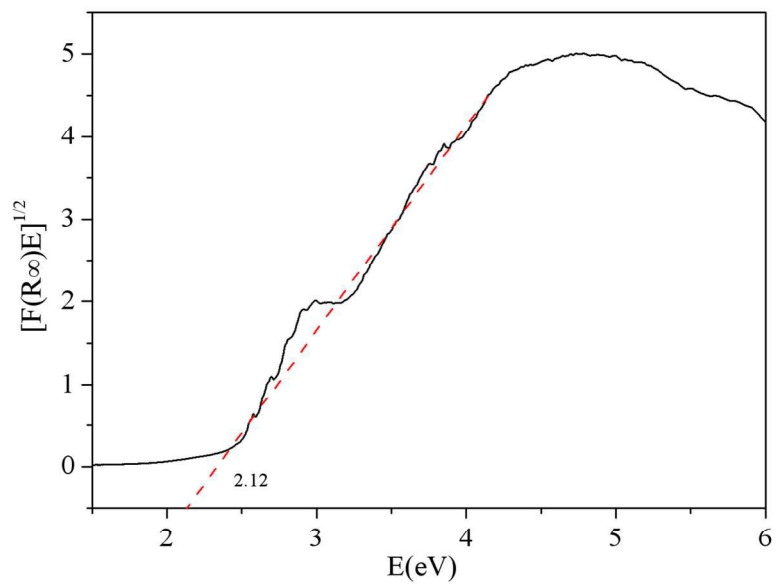
262x396mm (150 x 150 DPI)



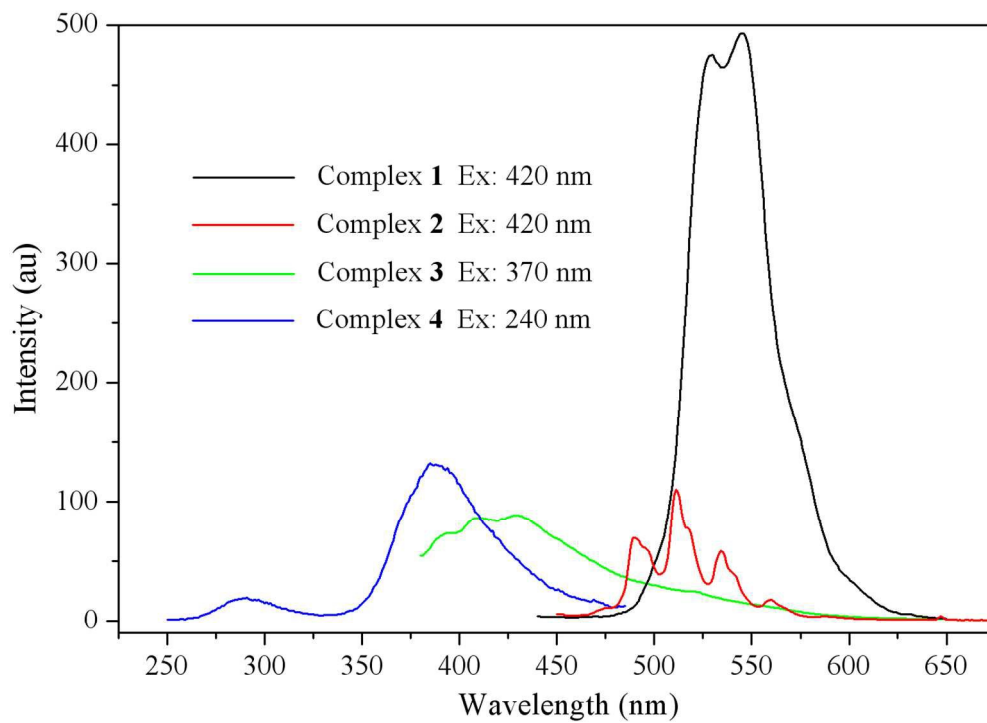
286x388mm (150 x 150 DPI)



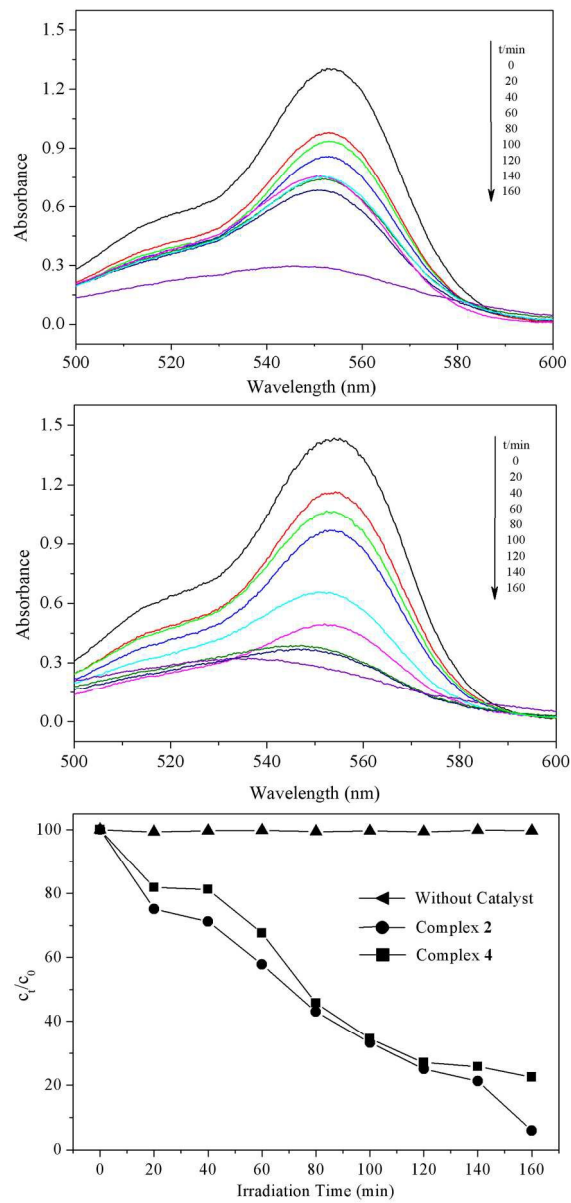
222x467mm (150 x 150 DPI)



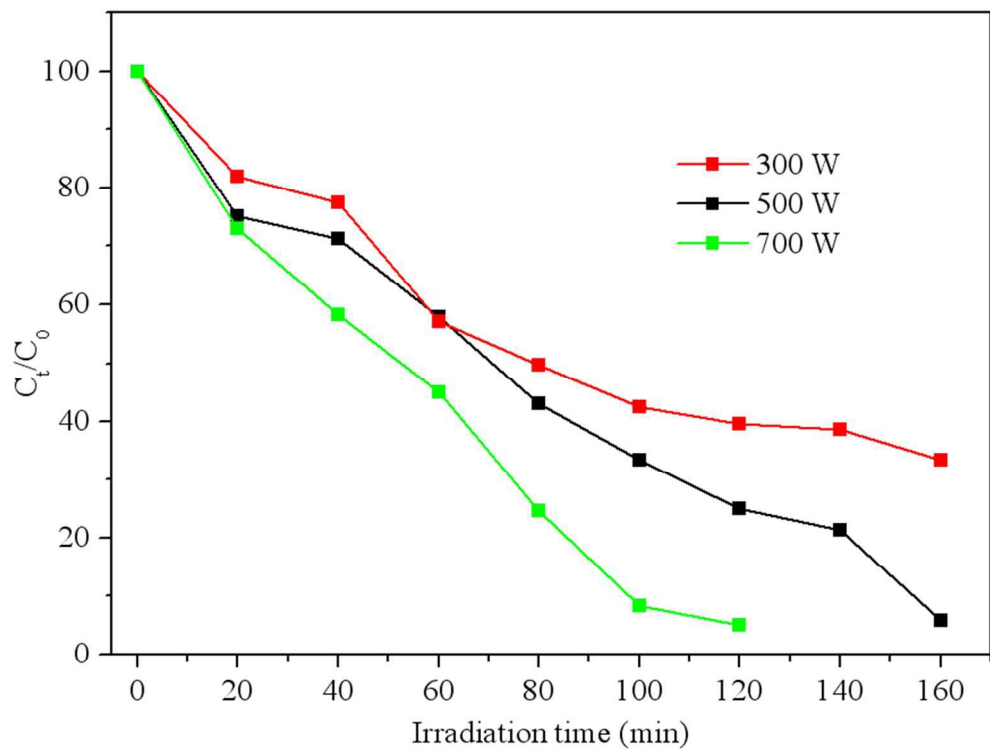
232x351mm (150 x 150 DPI)



247x178mm (150 x 150 DPI)



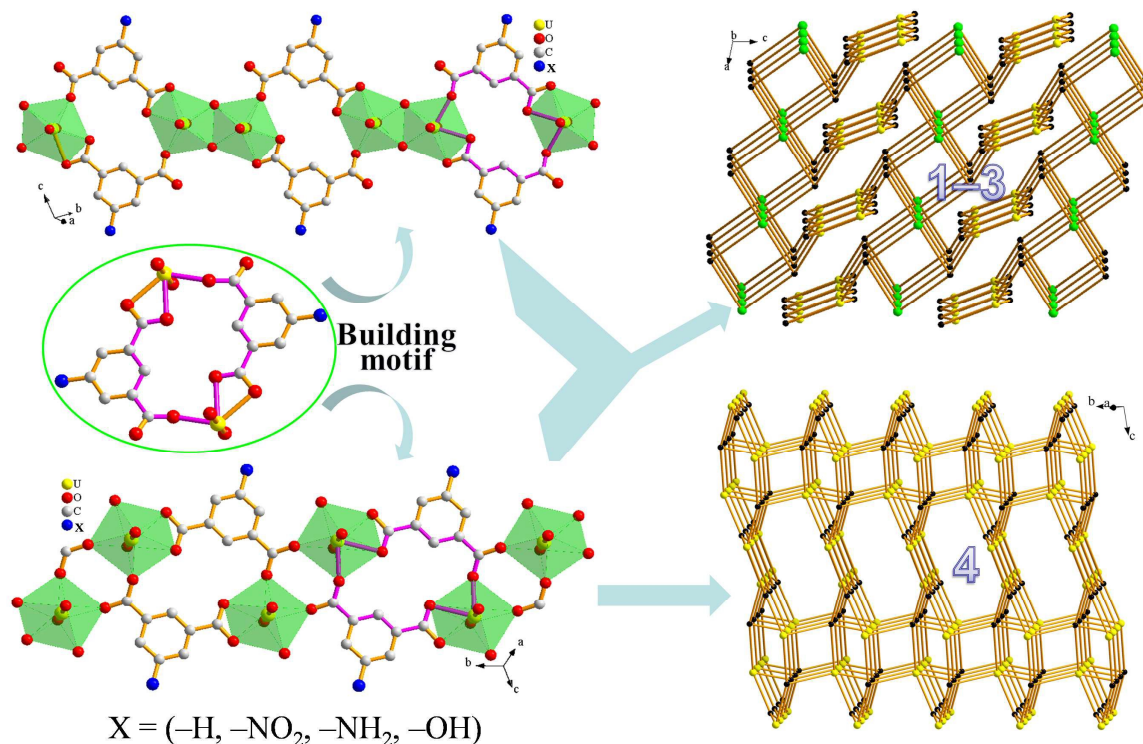
235x497mm (150 x 150 DPI)



149x112mm (150 x 150 DPI)

Graphic abstract

Pictogram



Synopsis

A family of 3D uranyl hybrid materials based 5-X-1,3-dicarboxylate ($X = -\text{H}, -\text{NO}_2, -\text{NH}_2, -\text{OH}$), $[(\text{UO}_2)_2(\text{H}_2\text{O})(\text{ipa})_2]$ (1), $[(\text{UO}_2)_2(\text{H}_2\text{O})(\text{nip})_2] \cdot \text{H}_2\text{O} \cdot \text{Et}_3\text{NH}$ (2), $[(\text{UO}_2)_2(\text{H}_2\text{O})(\text{aip})_2] \cdot \text{Et}_3\text{NH}$ (3) and $[(\text{UO}_2)(\text{hip})]_2 \cdot \text{H}_2\text{O}$ (4), have been synthesized. In which two types of 1D chains assembled by the same uranyl dimer motif $[(\text{UO}_2)_2\text{L}_2]$ through two different arrangement modes exist. And the structural analysis reveals four complexes exhibit two different topologies. The impact of the different substituent group on the acid ligands to the 3D structural morphology of four complexes is studied by the structural analysis and fluorescence spectra. 2 and 4 prove useful to degrade RhB under the irradiation of simulate daylight by 500 W xenon lamps, showing two compounds could be potential photocatalysts.